Journal of Power Sources 196 (2011) 6794–6801

Contents lists available at ScienceDirect

Journal of Power Sources

journal homepage: www.elsevier.com/locate/jpowsour

Investigation and application of lithium difluoro(oxalate)borate (LiDFOB) as additive to improve the thermal stability of electrolyte for lithium-ion batteries

Mengqing Xu[a,b], Liu Zhou[b], Liansheng Hao[a], Lidan Xing[a], Weishan Li[a,*], Brett L. Lucht[b]

[a] School of Chemistry & Environment and Key Lab. of Technology on Electrochemical Energy Storage and Power Generation in Higher Education Guangdong Institutes, South China Normal University, Guangzhou 510006, China
[b] Department of Chemistry, University of Rhode Island, Kingston, RI 02881, USA

ARTICLE INFO

Article history:
Received 26 August 2010
Received in revised form 6 October 2010
Accepted 18 October 2010
Available online 26 October 2010

Keywords:
Lithium difluoro(oxalate)borate
Electrolyte additive
Thermal stability
Elevated temperature
Lithium-ion battery

ABSTRACT

Lithium difluoro (oxalate) borate (LiDFOB) is used as thermal stabilizing and solid electrolyte interface (SEI) formation additive for lithium-ion battery. The enhancements of electrolyte thermal stability and the SEIs on graphite anode and $LiFePO_4$ cathode with LiDFOB addition are investigated via a combination of electrochemical methods, nuclear magnetic resonance (NMR), X-ray photoelectron spectroscopy (XPS), Fourier transform infrared-attenuated total reflectance (FTIR-ATR), as well as density functional theory (DFT). It is found that cells with electrolyte containing 5% LiDFOB have better capacity retention than cells without LiDFOB. This improved performance is ascribed to the assistance of LiDFOB in forming better SEIs on anode and cathode and also the enhancement of the thermal stability of the electrolyte. LiDFOB-decomposition products are identified experimentally on the surface of the anode and cathode and supported by theoretical calculations.

1. Introduction

While commercial lithium-ion batteries (LIBs) perform well for most home electronics applications, currently available LIB technology dose not satisfy some of the performance goals for Hybrid Electric Vehicles (HEV) or Plug-in Hybrid Electric Vehicles (PHEV). One of the significant problems with current LIBs is their poor stability to high temperatures and extended cycling. The most extensively used LIB electrolytes are composed of $LiPF_6$ dissolved in organic carbonates or esters [1,2]. However, $LiPF_6$ electrolytes have poor thermal stability and the required use of EC limits low temperature performance. Significant energy fading occurs after several years at room temperature and over a few months at moderately elevated temperatures (>55 °C) [3–5]. While there are several different factors that limit the thermal stability and calendar life of LIBs, the thermal stability of electrolyte at elevated temperature and the reactions of the electrolyte with the surface of the electrode materials are frequently reported to be the most important [6,7].

It is generally acknowledged that there are two effective methods to improve the thermal stability and high temperature performance of lithium-ion batteries. One is introduction of novel SEI formation additives to control the properties of electrode/electrolyte interfaces, and the other is the utilization of Lewis bases to inhibit the dissociation of $LiPF_6$ at elevated temperature [8–10]. As respect to the SEI formation additives, vinylene carbonate (VC) is one of the most widely investigated additives since it can form a more stable SEI film on the surface of the graphite anode than the electrolyte solvents [11–13]. However, VC is not a stable compound because it tends to polymerize, which may restrict its application. Lewis bases such as dimethyl acetamide (DMAc) stabilize $LiPF_6$ electrolytes by capturing the Lewis acidic PF_5 generated during the thermal dissociation of $LiPF_6$ [7]. The inhibition of the thermal decomposition of $LiPF_6$ electrolyte via addition of DMAc subsequently protects the anode SEI by preventing the formation of reactive species that degrade the SEI.

Lithium bis(oxalate)borate (LiBOB) has been reported as an alternative salt for improving electrolyte thermal stability of LIBs [14,15]. LIBs with LiBOB-based electrolytes have been reported to operate at 60 °C for 200 cycles with litter capacity fade [14]. This improvement is due to the presence of a stable solid electrolyte interface (SEI) formed by the ring-open reaction of the oxalate moiety and formation of trigonal borates at about 1.7 V vs Li/Li^+ [15–21]. In addition, previous investigations suggest that low concentration of LiBOB can significantly improved the thermal stability of electrolytes. However, the thick SEI layer formed in LiBOB-based electrolytes dramatically increases the interfacial impedance of the negative electrodes, therefore the power capability of the lithium-ion batteries is greatly deteriorated. Moreover, cells with LiBOB-based electrolytes have lower capacity and power

* Corresponding author. Tel.: +86 20 39310256; fax: +86 20 39310256.
E-mail address: liwsh@scnu.edu.cn (W. Li).

0378-7753/$ – see front matter © 2010 Elsevier B.V. All rights reserved.
doi:10.1016/j.jpowsour.2010.10.050

at low temperatures due to the lower ionic conductivity and higher resistance of interfacial impedance.

Alternatively, lithium difluoro (oxalate) borate (LiDFOB) has been reported as a novel salt for lithium-ion batteries with better cycling performance at elevated temperatures [22,23]. It is found that the impedance of cells with LiDFOB-based electrolytes is much lower than cells with LiBOB-based electrolytes since two fluoride atoms substitute the oxalate moieties of LiBOB salt. To our knowledge, there has been no report about the impacts of LiDFOB on the thermal stability of electrolyte and the interface of $LiFePO_4$/electrolyte at elevated temperature. In this report, the thermal stability of the electrolyte with LiDFOB salt added and its synergistic effect with $LiPF_6$ in carbonate solvents at elevated temperature were investigated with nuclear magnetic resonance (NMR). The effects of electrolyte with LiDFOB added on $LiFePO_4$ electrode and graphite electrodes at elevated temperature were also investigated by using X-ray photoelectron spectroscopy (XPS) and Fourier transform infrared-attenuated total reflectance (FTIR-ATR). Density functional theory (DFT) calculations have also been performed to interpret LiDFOB-decomposition products at the interfaces.

2. Experimental

Battery-grade carbonates were purchased from Tinci Company (Guangzhou Tinci Materials Technology Co. Ltd., China) and used without further purification. Battery-grade lithium hexafluorophosphate ($LiPF_6$) was obtained from Hashimoto Chemical Corporation and used without further purification. Lithium difluoro (oxalate) borate (LiDFOB) was purchased from the company (Fujian Chuangxin Science and Technology Development Co. Ltd., China) and used without further purification. The composition of the electrolyte used in all of the cells was a 1.0 M $LiPF_6$ solution in EC/DMC/DEC (1/1/1, v/v/v) (STD) with and without LiDFOB salt (5 wt.%). Water and free acid (HF) contents in the electrolyte were controlled to be less than 20 ppm and 50 ppm, respectively, determined by Karl-Fisher 831 Coulometer (Metrohm) and Karl-Fisher 798 GPT Titrino (Metrohm).

Samples for NMR spectroscopy were prepared in an Ar-filled glove box followed by flame sealing and storage for varying lengths of time at 85 °C. NMR analyses were conducted on a JEOL 400 MHz NMR spectrometer. ^{19}F NMR resonances were referenced to $LiPF_6$ at 65.0 ppm, ^{31}P NMR resonances were referenced to $LiPF_6$ at −145.0 ppm, and ^{11}B NMR resonances were referenced to LiBOB at 6.6 ppm.

Pounch cells were fabricated with $LiFePO_4$ as cathode and graphite as anode and Celgard 2325 separators. The anode electrodes contained 95% graphite, 1% acetylene carbon black, 1.5% carboxymethyl cellulose (CMC) and 2.5% styrene butadiene rubber (SBR); cathode electrodes contained 90% $LiFePO_4$, 5% acetylene carbon black, and 5% binder. $LiFePO_4$ and graphite are provided by Shenzhen BTR new energy materials Co. Ltd., China. The capacity ration for cathode electrode and anode electrode is 1:1.3. The cells were cycled with a constant-current–constant-voltage charge and a constant-current discharge of 1 C rate between 3.85 V and 2.0 V using BS-9300R type battery cycle (Guangzhou, China).

The graphite anodes and $LiFePO_4$ cathodes were washed with anhydrous DMC solvent 3 times to remove residual EC and $LiPF_6$ salt followed by vacuum drying overnight at room temperature. The XPS spectra were carried out with a Kratos Axis Ultra spectrometer, using a focused monochromatized Al Kα radiation ($h\upsilon$ = 1486.6 eV). Lithium was not monitored due to its low inherent sensitivity and small change of binding energy. Calibration of XPS peak position was made by recording XPS spectra for reference compounds, which would be presented on the electrode surfaces: LiF, Li_2CO_3, $Li_xPO_yF_z$ and lithium alkyl-carbonate. The graphite peak at 284.3 eV was used as a reference for the final adjustment of the energy scale in the spectra. The spectra obtained were fitted using XPS peak software (version 4.1). Line syntheses of elemental spectra were conducted using a Guassian–Lorentzain (70:30) curve fit with Shirley background subtraction. The element concentration was calculated based on the equation $C_x = (I_x/S_x)/(\sum I_i/S_i)$, where I_x is the intensity of the relative element and S_i is the sensitivity number of the element. Fourier transform infrared-attenuated total reflectance (FTIR-ATR) analysis of the anode and cathode electrodes was carried out with a Bruker Tensor 27 spectrometer, with germanium crystal and 4 cm^{-1} resolution and 64 scans.

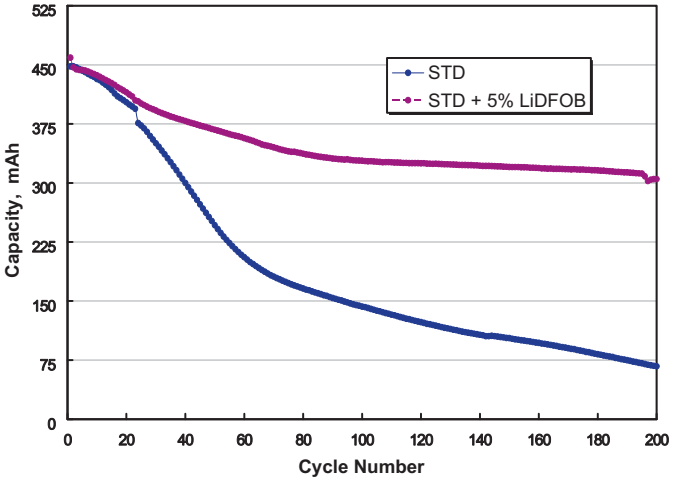

Fig. 1. Cycling performance of $LiFePO_4$/graphite cells with and without LiDFOB (5 wt.%) electrolyte at 60 °C.

All calculations were performed on Gaussian 03 package [24]. The equilibrium state structure are optimized by B3LYP method at 6-311++G(d,p) basis set. To confirm each optimized stationary point and make zero-point energy (ZPE) corrections, frequency analyses were done with the same basis set. Charge distribution is analyzed by the natural bond orbital (NBO) theory.

3. Results and discussion

3.1. Cycling performance of cells with and without LiDFOB electrolyte

Pounch cells were constructed containing STD and STD with 5% LiDFOB electrolytes. Fig. 1 shows cyclic performances of $LiFePO_4$/graphite cells with STD and STD with 5% LiDFOB electrolytes at 60 °C. Cells containing STD electrolyte experience a discharge capacity drop from 448 mAh on the first cycle to 67.2 mAh on the 200th cycle at 60 °C. The capacity retention is about 15%. When STD with 5% LiDFOB electrolyte is used the capacity drops from 459.1 mAh on the first cycle to 304.9 mAh on the 200th cycle, or about 66.4% retention of the original capacity. This suggests that addition of 5% LiDFOB can significantly improve the cycling stability at elevated temperature. Thermal stability of the electrolytes with LiDFOB, as well as surface analyses of electrodes extracted from cells with and without LiDFOB, as described below, provide insight into the sources of the difference in capacity retention at elevated temperature.

3.2. Thermal stability of the electrolyte with LiDFOB addition

The thermal stability of $LiPF_6$ in carbonate solvents has been reported in previous literatures [25,26]. Storage of $LiPF_6$-base carbonate electrolytes at elevated temperature results in the thermal dissociation of $LiPF_6$ to LiF and PF_5. The Lewis acidic PF_5

reacts rapidly with trace protic impurities in the electrolyte, such as ROH or H_2O, to form OPF_3, which then initiates an autocatalytic decomposition of the electrolyte. Previous investigations of $LiPF_6$/carbonate electrolytes indicate nearly quantitative decomposition upon storage for several days at 85 °C, forming a number of by-products, including CO_2, alkyl ethers (R_2O), alkylfluorides, phosphorus oxyfluoride (OPF_3), and fluorophosphates [OPF_2OR, $OPF(OR)_2$].

However, upon incorporation of 5% LiDFOB to $LiPF_6$/carbonate electrolyte the thermal decomposition is dramatically inhibited. Fig. 2 shows the ^{19}F, ^{31}P and ^{11}B NMR spectra of 1.0 M $LiPF_6$/EC:DMC:DEC electrolyte with 5% (wt.) LiDFOB before and after thermal storage at 85 °C for 2 months. Storage of ternary electrolyte with 5 wt.% LiDFOB added at 85 °C for 2 months results in the appearance of new species observed in NMR spectroscopy. Analyses of ^{19}F and ^{11}B NMR spectra are consistent with the generation of new species including $LiBF_4$. $LiBF_4$ is characterized by resonances at −17.1 ppm in ^{19}F and −2.3 ppm in ^{11}B NMR spectra. In addition to the resonances of $LiPF_6$, $LiBF_4$, and LiDFOB, there is another set of resonances in the ^{19}F and ^{31}P NMR spectra. The additional resonances consist of two doublets of triplets at 79.7 ppm (776 Hz, 52 Hz) and 62.8 ppm (748 Hz, 52 Hz) in ^{19}F NMR spectra and a triplet of triplets at −142.3 ppm (776 Hz, 748 Hz) in ^{31}P NMR spectra. We attribute to the new resonances to an anion with two pairs of chemically inequivalent fluorine atoms and a single oxalate ligand attached to phosphorus, lithium tetrafluorooxaltophosphate ($LiPF_4C_2O_4$) [27–29].

The generation of $LiBF_4$ and $LiPF_4C_2O_4$ results from disproportionation reactions of $LiPF_6$ with LiDFOB. The fluoride ligands on phosphorus are exchanged with oxalate ligands on boron. Analysis of ^1H NMR spectrum suggests that no decomposition of carbonate solvents took place after thermal storage at 85 °C for 2 months, consist with the ^{13}C NMR spectrum and GC-MS results. In addition, only small set of resonances characteristic of $OPF_2(OLi)$ (^{19}F, δ = 54.4 ppm, d, $J_{P\text{-}F}$ = 988), LiF/FH (^{19}F, ∼ −10 ppm) are observed after 2 months thermal storage. Continued storage at 85 °C for over 6 months only results in only small changes to the spectra suggesting that the thermal decomposition reactions are significantly inhibited. This suggests that the addition of LiDFOB to $LiPF_6$-based electrolytes inhibits the autocatalytic thermal decomposition of the electrolyte. The enhanced thermal stability of the $LiPF_6$-based electrolyte is attributed to the Lewis basic oxalate ligand, sequestering PF_5 generated during the thermal dissociation of $LiPF_6$. Similar disproportionation reactions are observed upon the thermal storage of ternary electrolyte with 5 wt.% LiBOB [27].

3.3. X-ray photoelectrons spectroscopy (XPS) analyses of graphite electrode

In order to better understand the sources of superior capacity retention of cells containing STD and STD with 5% LiDFOB electrolyte, the cells after 200 cycles at 60 °C were disassembled in an argon filled glove box and the surfaces of the electrodes were analyzed by XPS. Analyses of the anodes reveal significant differences in the surface species (Fig. 3, Table 1). The concentrations of C is decreased for both cycled anodes while the concentrations of O, F, P are increased compared to the fresh anode electrode. As respect to the graphite anode cycled with 5% LiDFOB containing electrolyte, the B element could be detected at the surface of the electrode. This suggests the active electrode material is covered by a SEI film. The concentrations of C and O are higher for the anode cycled with 5% LiDFOB containing electrolyte than those for the anode with STD electrolyte. However, the concentrations of F and P are much lower for the anode cycled with 5% LiDFOB containing electrolyte than those for the anode with STD electrolyte.

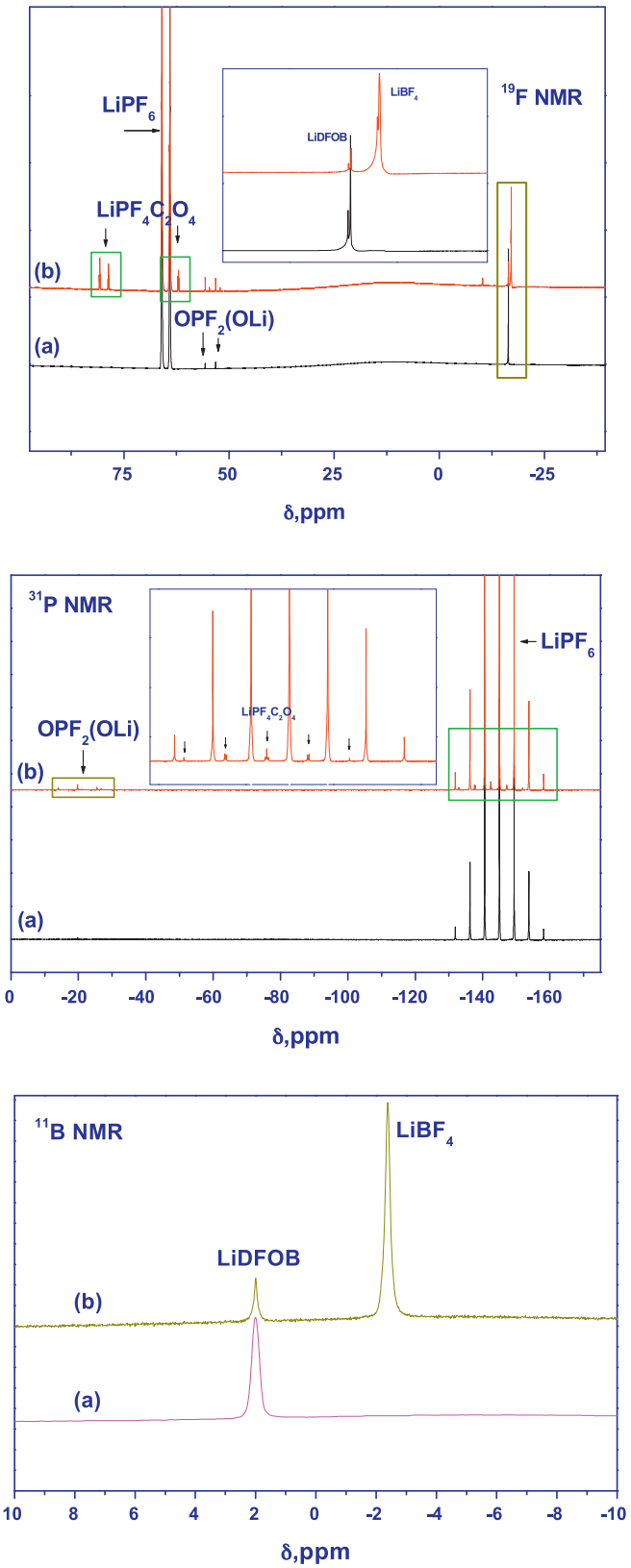

Fig. 2. ^{19}F, ^{31}P and ^{11}B NMR spectra of LiDFOB containing electrolyte, (a) before thermal storage and (b) storage at 85 °C for 2 months.

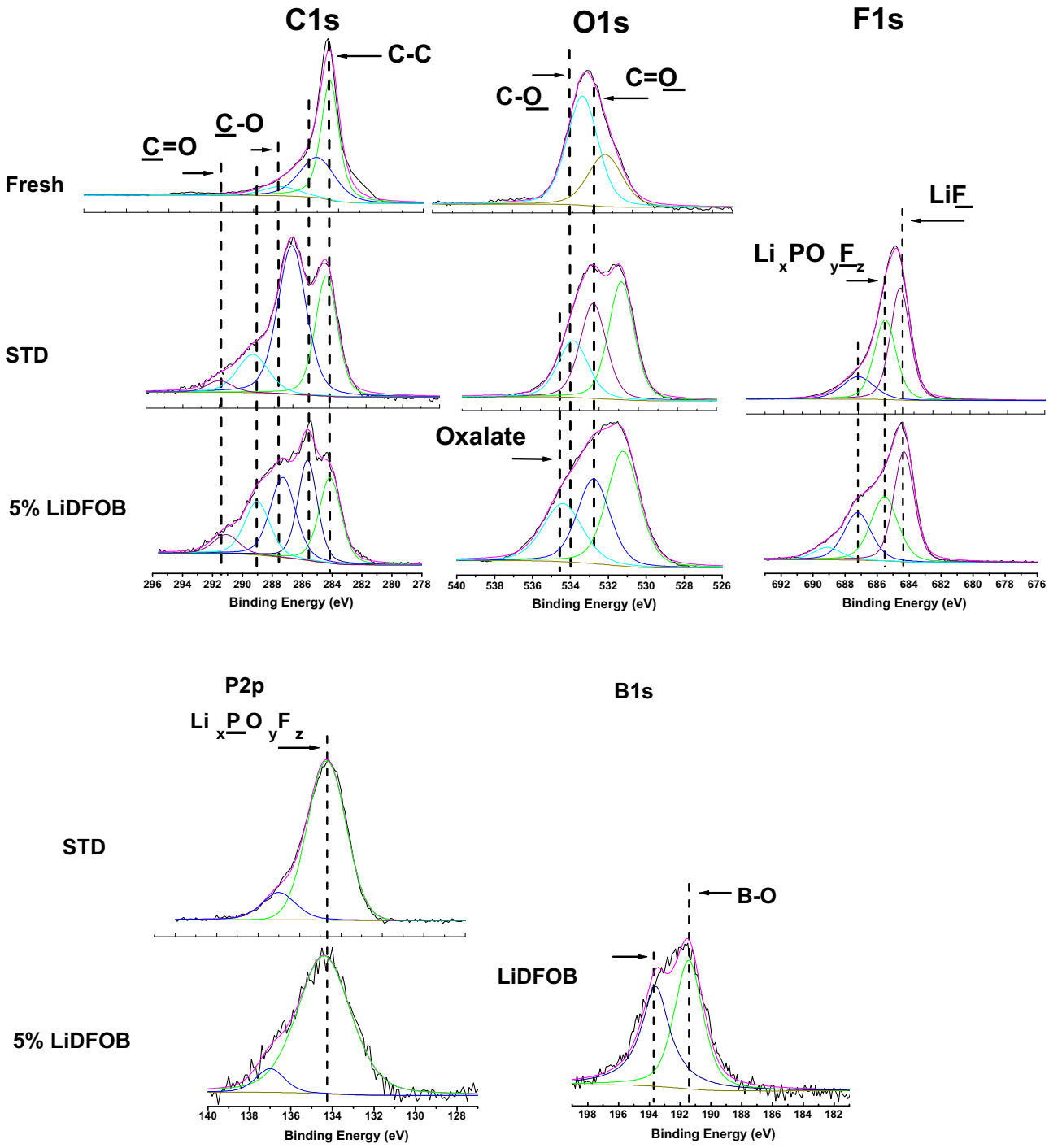

Fig. 3. C 1s, O 1s, F 1s, P 2p and B 1s XPS spectra of fresh graphite anode and cycled with STD and STD + 5% LiDFOB (wt.) electrolyte at 60 °C for 200 cycles.

The C 1s spectrum of the fresh anode consists of three peaks. The first one at 284.3 eV is attributed to graphite [30,31]. The second one at 285.0 eV is assigned to SBR binder and also to hydrocarbon contamination, while the peaks observed at 286.7 eV is attributed to the C–O like carbon atoms in the CMC binder [32]. After 200 cycles at 60 °C, the C 1s spectrum of the anode cycled with STD electrolyte contains four peaks characteristic of graphite (284.3 eV), C–O bonds in ethers or carbonates (286 eV), C=O bonds in lithium alkyl carbonates and polycarbonates (290 eV), as well as Li_2CO_3 (291 eV). The peak at 285 eV corresponding to SBR binder has disappeared, which suggests the electrode surface has been covered by a thick SEI film. The C 1s spectrum of the anode cycled with LiDFOB electrolyte contains peaks at 286–288 eV, consistent with the presence of C–O bonds in esters and carbonates, C=O bonds in lithium alkyl carbonates and polycarbonates (290 eV), Li_2CO_3 (291.0 eV), as well as graphite (284.3 eV). In addition, a peak at 289 eV is present, char-

Table 1
Surface concentrations of different elements on fresh anode and anode from cycled cells with STD electrolyte and with LiDFOB containing electrolyte.

Sample	C 1s (%)	O 1s (%)	F 1s (%)	P 2p (%)	B 1s (%)
Fresh	82.8	14.7	2.5		
STD electrolyte	19.9	22.6	50	7.5	
STD + 5% LiDFOB	30.1	35.4	23.7	4.2	6.6

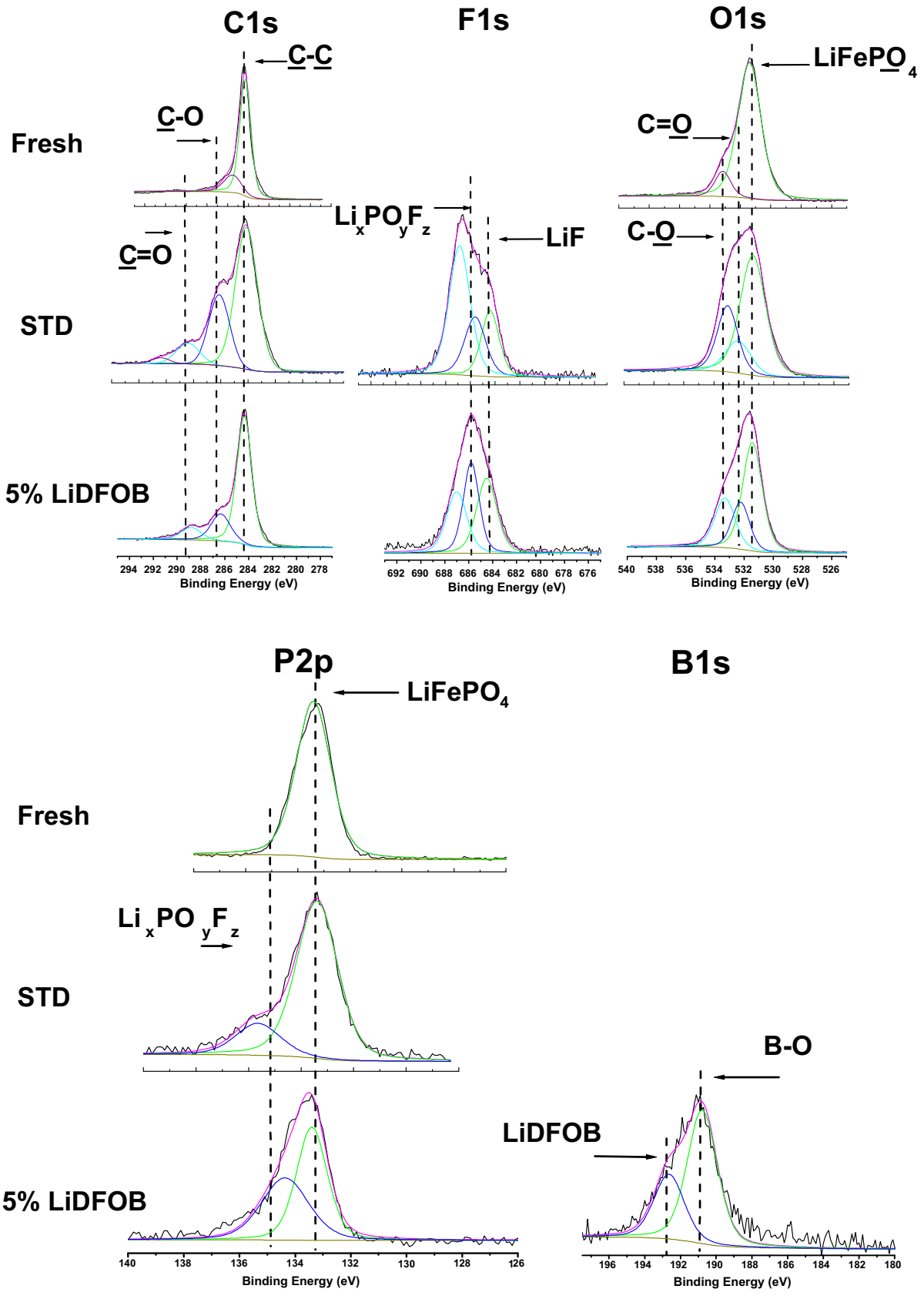

Fig. 4. C1s, O1s, F1s, P2p and B1s XPS spectra of fresh $LiFePO_4$ cathode and cycled with STD and STD + 5% LiDFOB (wt.) electrolyte at 60 °C for 200 cycles.

acteristic of oxalate, corresponding to the decomposition products of LiDFOB at graphite anode [16].

The O 1s spectrum of the fresh anode consists of two main peaks assigned to the oxygen atoms of the CMC binder. For the anode cycled with STD electrolyte and LiDFOB containing electrolyte at 60 °C, we can observed that the replacement of the O 1s components of the CMC binder by new components, which shows the deposition of new oxygenated species. The O 1s spectrum of the anode cycled with the STD electrolyte contains a broad peak characteristic of C–O and C=O containing components at 532–533.5 eV. This suggests the deposition of carbonate salts, lithium alky carbonates $ROCO_2Li$, or polycarbonates on the surface of the electrode, resulting from the decomposition of the solvents and salt [33]. Several formation mechanisms of the carbonate species can be found in the literatures [34,35]. The O 1s spectrum of the anode cycled containing STD with 5% LiDFOB electrolyte is slightly different from that of the anode containing STD electrolyte. In addition to C–O and C=O, as well as Li_2CO_3 (531.5 eV) peaks observed with the STD electrolyte, a new peak at ~533.7 eV is observed. This peak is associated to the oxalate species, resulting from the degradation of LiDFOB, and correlated to the C 1s peak at ~288 eV, discussed above [16].

The F 1s spectrum of the anode cycled with STD electrolyte at 60 °C shows three main peaks. The peak at 684.5 eV and 685.7 eV, attributed to LiF and $Li_xPO_yF_z$, respectively, decomposition products of $LiPF_6$ commonly observed at electrode/electrolyte interface at elevated temperature. An additional peak in F 1s at 687 eV is attributed to the remaining salt $LiPF_6$, despite washing the electrode with DMC before XPS analysis. The F 1s spectrum of the anode extracted from a cell containing STD with 5% LiDFOB is similar but the intensity of $Li_xPO_yF_z$ is much lower than that of the anode cycled with the STD electrolyte, as also supported from Table 1.

The P 2p spectra of the two samples are very similar, showing two peaks at about 134.5 eV and 137 eV, the peak at 134.5 eV is characteristic of $Li_xPO_yF_z$, and the peak at 137 eV could be assigned to Li_xPF_y.

As respect to the anode cycled with STD with 5% LiDFOB electrolyte, two peaks can be detected in B 1s spectrum, which confirms that B is incorporated into the structure of SEI. The peak at 191.5 eV could be assigned to the decomposition product of $LiBF_2C_2O_4$, consistent with the ring opening process of $LiBF_2C_2O_4$ and the generation of $Li_xBO_yF_z$ species [7,16], which corrected to the C 1s peak at ~288 eV and O 1s ~533.7 eV, discussed above, and also supported by the DFT calculations, as discussed below. The other peak at 193.8 eV is attributed to the remaining salt $LiBF_2C_2O_4$.

3.4. X-ray photoelectrons spectroscopy (XPS) analyses of $LiFePO_4$ electrodes

The fresh $LiFePO_4$ cathode is characterized by peaks corresponding to the metal oxide, 531.4 eV in O 1s spectrum, 133.5 eV in P 2p spectrum, as well as Fe 2p spectrum. Because not too much differences were observed whether the cathode cycled with STD electrolyte or with 5% LiDFOB containing electrolyte, the Fe 2p is not shown here. The Fe 2p spectrum is split into two parts due to spin–orbit coupling (Fe 2p3/2 and Fe 2p1/2) with an intensity ration of about 2/1 [32]. The peak at 284.3 eV in C 1s is attributed to the black carbon. An additional peak at ~285 eV in C 1s of the fresh $LiFePO_4$ is also present, characteristic of the binder.

Analysis of the cathode surface reveals significant differences between the cells cycled with STD electrolyte and LiDFOB containing electrolyte after 200 cycles at 60 °C (Figs. 4 and 5, Table 2). Compared to the fresh cathode electrode, the concentrations of C and Fe are decreased for both cycled cathodes, while the concentrations of O and F are increased. The concentration of P is slightly increased for the cathode cycled with STD electrolyte, but

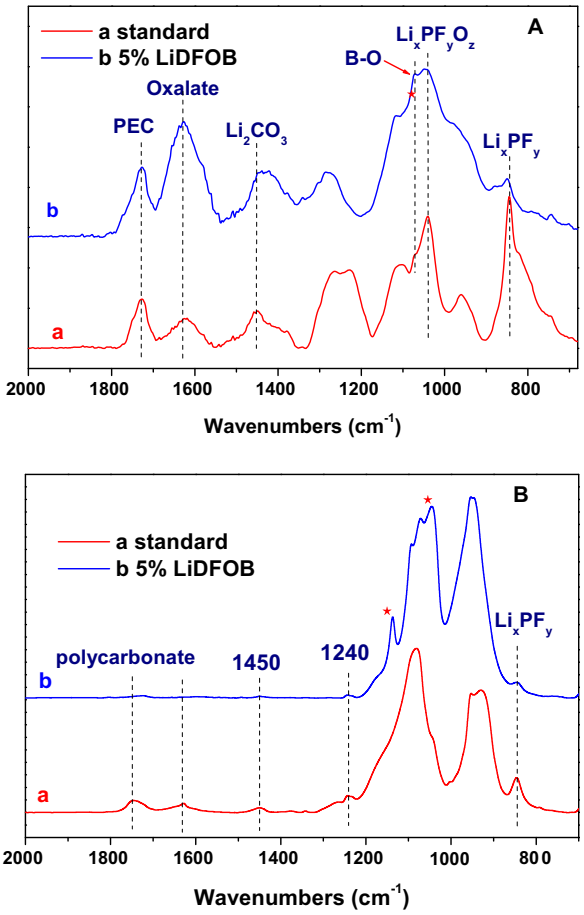

Fig. 5. FTIR-ATR spectra of the graphite (A) and $LiFePO_4$ (B) electrodes cycled at 60 °C after 200 cycles with and without 5% LiDFOB added.

decreased for the cathode cycled with LiDFOB containing electrolyte. For the cathode cycled with LiDFOB containing electrolyte, B element could also be detected in B 1s spectrum. This suggests that the $LiFePO_4$ cathode surface is also covered a SEI layer, and also confirms that B is incorporated into structure of SEI formed on the cathode surface.

The C 1s spectra are very similar and dominated by graphite (284.3 eV), C=O bonds in lithium alkyl carbonates ($R–CH_2OCO_2–Li$) and polycarbonates, as well as C–O bonds in ethers or carbonate salts (286–287 eV). However, the intensity of C=O and C–O observed on the surface of the $LiFePO_4$ electrode cycled with STD electrolyte is slightly stronger than that of the cathode cycled with the LiDFOB containing electrolyte (Fig. 4, Table 2). This suggests that the $LiFePO_4$ cathode electrode cycled with STD electrolyte was covered more degradation products of electrolyte than that of the electrode cycled with LiDFOB containing electrolyte, which is consistent with the FTIR data, as discussed below.

The O 1s spectra have some similar peaks presence, containing the lithium metal oxide, $LiFePO_4$ (531.4 eV), C–O bonds in polycarbonates and carbonate salts (533.5 eV), as well as C=O bonds in

Table 2
Surface concentrations of different elements on fresh $LiFePO_4$ cathode and cathode from cycled cells with STD electrolyte and with LiDFOB containing electrolyte.

Sample	C 1s (%)	O 1s (%)	F 1s (%)	P 2p (%)	Fe 2p (%)	B 1s (%)
Fresh	60.1	22.3	0.9	7.9	8.8	
STD electrolyte	49.8	28.6	8.6	8.2	4.8	
STD + 5% LiDFOB	50.1	25.6	7.2	6.7	4.9	5.5

ethers and carbonate salts (532.5 eV), which is the products from electrolyte degradation. However, the passivating layer remains very thin ever after 200 cycles at 60 °C since the intensity of $LiFePO_4$ (531.4 eV) almost unchanged for the two samples, showing that the surface of $LiFePO_4$ particles is not very reactive toward the electrolyte at elevated temperature [32].

The F 1s spectra are similar and contain three peaks LiF (684.5 eV), $Li_xPO_yF_z$ (686 eV), as well as Li_xPF_y (687 eV). The P 2p spectra are dominated by $LiFePO_4$ (133.4 eV), and the deposition of a small amount of $Li_xPO_yF_z$ (135 eV). As respect to the cathode cycled with STD with 5% LiDFOB electrolyte, two peaks can be observed in B 1s spectrum. The peak at 191.2 eV could be assigned to the ring opening process of $LiBF_2C_2O_4$ and the generation of tri-coordinated borates or $Li_xBO_yF_z$ species [7,16], which correlated to the C 1s peak at ~288 eV and O 1s ~533.7 eV, discussed above. The other peak at 193. 2 eV is attributed to the deposition salt of $LiBF_2C_2O_4$ on the cathode surface.

3.5. FTIR-ATR

Analysis of the graphite anodes (Fig. 5A) and $LiFePO_4$ cathodes (Fig. 5B) by FTIR-ATR spectra provides additional insight into the differences of electrodes surface after 200 cycles at 60 °C with and without LiDFOB added. The IR spectra of the anodes extracted from cells containing different electrolytes are similar and are dominated by the absorptions characteristics of polycarbonate (1730 cm^{-1}), Li_2CO_3 (~1500 cm^{-1}), $Li_xPO_yF_z$ (1039 cm^{-1}), Li_xPF_y (843 cm^{-1}) besides the binder peaks [16,36,37]. In addition, the electrodes extracted from the cells with LiDFOB added electrolytes contain additional peaks at 1071 and 1630 cm^{-1}, characteristics of B–O species and oxalate. Irreversible reaction of LiDFOB on the electrode surface is most likely the source of the differences.

As respect to the cathode electrode, the IR spectra are similar and are dominated by the binder peaks. In addition, the polycarbonate (1730 cm^{-1}) and Li_xPF_y (843 cm^{-1}) are also presented. However the cathode cycled with the standard electrolyte has stronger polycarbonate absorption at 1730 cm^{-1}. This suggests that addition LiDFOB inhibits the decomposition of the electrolyte at elevated temperature. In addition, the $LiFePO_4$ cathode electrodes extracted from the cells with LiDFOB containing electrolyte have absorptions characteristic of B–O–B, and B–F linkages (1041, 1141 cm^{-1}), related to tri-coordinated borates or $Li_xBF_yO_z$ in the SEI, which is consistent with the XPS data, and also supported by the DFT calculations, as discussed below.

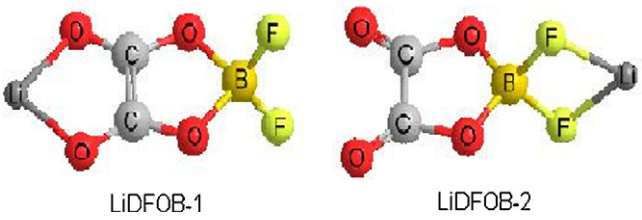

Fig. 6. The optimized geometry of LiDFOB in gas phase at B3LYP/6-311++G(d,p) level.

3.6. DFT calculations on the decomposition of LiDFOB

3.6.1. Optimized structure of LiDFOB

The optimized geometry and selected structural parameter of LiDFOB in gas phase at B3LYP/6-311++G(d,p) level are presented in Fig. 6. Two different structures are acquired since Li could coordinate with oxygen atoms or fluoride atoms, as labeled LiDFOB-1 and LiDFOB-2, respectively. Both of the two geometries have the C 2v symmetry. However, the relative energy of LiDOB-1 is slightly lower than that of LiDFOB-2, −609.66 a.u. and −609.64 a.u., respectively, which suggests that LiDFOB-1 is more stable than LiDFOB-2.

3.6.2. Decomposition mechanism of LiDFOB in gas phase

The initial reductive decomposition of LiDFOB (1) involves one electron transfer from anode to LiDFOB, resulting in radical anion $[LiDFOB]^-$ (2). The ring-opening reaction of the radical anion $[LiDFOB]^-$ proceeds via the transition state $[LiDFOB]^-$-TS (3), the energy barrier is approximately 145.6 kJ mol^{-1} in the gas phase. Frequency analysis shows only one imaginary frequency (−72) corresponding to the transition state. With the presence of Li^+ cation,

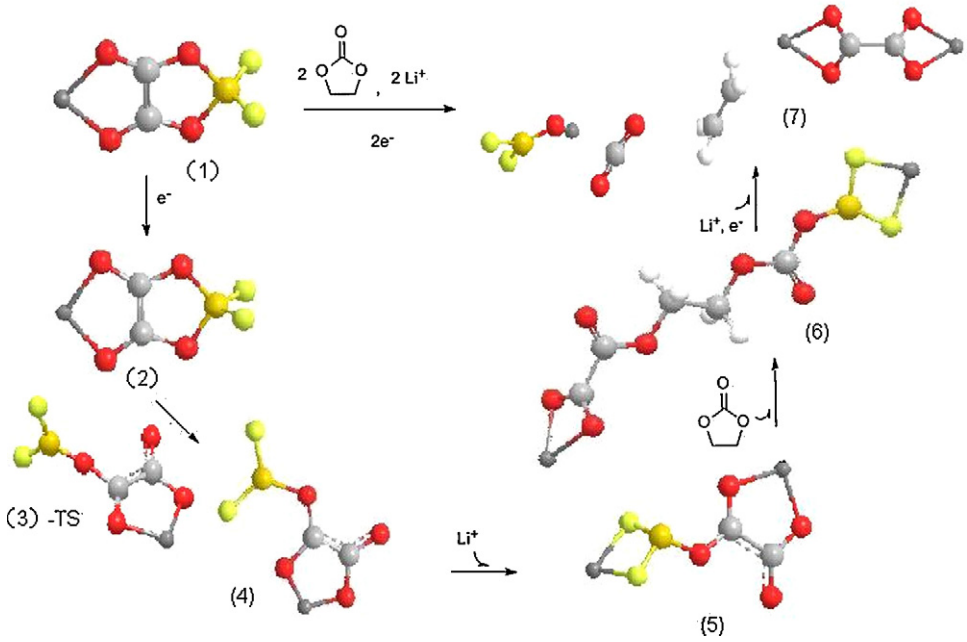

Fig. 7. Decomposition mechanism of LiDFOB and possible reaction process in gas phase.

Table 3
Relative energies, enthalpies, and free energies (in kJ mol^{-1}) of the stationary points, and imaginary frequency (ω) of the transition state for the reductive of LiDFOB.

Structure	ΔE	$\Delta E + \Delta ZPE$	ΔH	ΔG	ω
LiDFOB (1)	0.0	0.0	0.0	0.0	
LiDFOB + e$^-$ (2)	−123.8	−128.6	−128.6	−130.6	
LiDFOB + e$^-$-ts (3)	26.9	17.0	18.0	10.9	72 *i*
LiDFOB + e$^-$-anion (4)	−481.1	−484.6	−484.2	−466.7	

the transition state [LiDFOB]$^-$-TS leads to the intermediate product (5). The intermediate product of B–O cleavage coupled with a ring-opening of EC generates another intermediate product (6). With the presence of Li^+ cation, the intermediate product (6) leads to the formation of $Li_2C_2O_4$, CO_2, C_2H_4, as well as a $Li(BF_2O)_n$ polymer. The calculated relative energy (ΔE), potential energy ($\Delta E + \Delta ZPE$), enthalpy (ΔH), and free energy (ΔG) of the stationary points are listed in Table 3. The possible reaction processes are proposed in Fig. 7.

4. Conclusions

Addition of 5% lithium difluoro (oxalate) borate (LiDFOB) to 1.0 M $LiPF_6$ EC/DMC/DEC (1/1/1, v/v/v) electrolyte can significantly improve the cyclic performance of $LiFePO_4$/graphite cells at 60 °C. The discharge capacity retention increased from 15% to 66.4% after 200 cycles under 60 °C. This can be ascribed to the enhancement of the thermal stability of the electrolyte containing 5% LiDFOB, and the formation of a stable SEI layer on both the anode and cathode electrodes in the presence of LiDFOB. The mechanisms of enhancements of thermal stability of the electrolyte and interface layers have been investigated by NMR, FTIR and XPS. It is found that the addition of LiDFOB to $LiPF_6$-based electrolytes inhibits the autocatalytic thermal decomposition of the electrolyte, generating of lithium tetrafluorooxaltophosphate ($LiPF_4C_2O_4$) due to the synergistic effect between LiDFOB and $LiPF_6$ at elevated temperature. It is also found that the formation of borates or its derivative products resulting from the degradation of LiDFOB on both the anode and cathode electrodes is also a leading factor for the improvement of the cycling performance at elevated temperature. DFT calculations provide additional support for the structure of the LiDFOB derived components on the electrode surface.

Acknowledgement

This work is supported by the National Natural Science Foundation of China (Nos. NSFC20873046, NSFC21003054), Natural Science Foundation of Guangdong Province (No. 10351063101000001), Specialized Research Fund for the Doctoral Program of Higher Education (Grant No. 200805740004), and Project of Guangdong Province (Grant No. 2009B050700039).

References

[1] PNGV Battery Test Manual Revision 2, August 1999, DOE/ID-10597.
[2] K. Xu, Chem. Rev. (Washington, D.C.) 104 (2004) 4304.
[3] M.C. Wu, P.J. Chiang, J.C. Liu, J. Electrochem. Soc. 152 (2005) A1041.
[4] A.M. Andersson, K. Edstrom, J. Electrochem. Soc. 148 (2001) A1100.
[5] H.Y. Xu, S. Xie, Q.Y. Wang, X.L. Yao, Q.S. Wang, C.H. Chen, Electrochim. Acta 52 (2006) 636.
[6] W. Li, B.L. Lucht, J. Electrochem. Soc. 153 (2006) A1617.
[7] S. Santee, A. Xiao, L. Yang, J. Gnanaraj, B.L. Lucht, J. Power Sources 194 (2009) 1053.
[8] M.Q. Xu, W.S. Li, B.L. Lucht, J. Power Sources 193 (2009) 804.
[9] J. Li, W.H. Yao, Y.S. Meng, Y. Yang, J. Phys. Chem. C 112 (2008) 3539.
[10] W. Li, C. Campion, B.L. Lucht, B. Ravdel, J. DiCarlo, K.M. Abraham, J. Electrochem. Soc. 152 (2005) A1361.
[11] D. Aurbach, K. Gamolsky, B. Markovsky, Y. Gofer, M. Schmidt, U. Heider, Electrochim. Acta 47 (2002) 1423.
[12] H. Ota, Y. Sakata, A. Inoue, S. Yamaguchi, J. Electrochem. Soc. 151 (2004) A1659.
[13] S.S. Zhang, K. Xu, T.R. Jow, Electrochim. Acta 51 (2006) 1636.
[14] K. Xu, U. Lee, S.S. Zhang, T.R. Jow, J. Electrochem. Soc. 151 (2004) A2106.
[15] W. Xu, C.A. Angell, Electrochem. Solid State Lett. 4 (2001) E1.
[16] A. Xiao, L. Yang, B.L. Lucht, S.–H. Kang, D.P. Abraham, J. Electrochem. Soc. 156 (2009) A318.
[17] K. Xu, S. Zhang, T.R. Jow, Electrochem. Solid State Lett. 8 (2005) A365.
[18] K. Xu, S. Zhang, B.A. Poese, T.R. Jow, Electrochem. Solid State Lett. 5 (2002) A259.
[19] C. Lee, B. Mun, P.N. Ross, Electrochem. J. Soc. 149 (2002) A1286.
[20] G.F. Ortiz, R. Alcantara, P. Lavela, J.L. Tirado, Electrochem. J. Soc. 152 (2005) A1797.
[21] G.V. Zhuang, P.N. Ross, Electrochem. Solid State Lett. 6 (2003) A136.
[22] S.S. Zhang, Electrochem. Commun. 8 (2006) 1423.
[23] Z. Chen, Y. Qin, J. Liu, K. Amine, Electrochem. Solid State Lett. 12 (2009) A69.
[24] M.J. Frisch, G.W. Trucks, H.B. Schlegel, G.E. Scuseria, M.A. Robb, J.R. Cheeseman, J.A. Montgomery Jr., T. Vreven, K.N. Kudin, J.C. Burant, J.M. Millam, S.S. Iyengar, J. Tomasi, V. Barone, B. Mennucci, M. Cossi, G. Scalmani, N. Rega, G.A. Petersson, H. Nakatsuji, M. Hada, M. Ehara, K. Toyota, R. Fukuda, J. Hasegawa, M. Ishida, T. Nakajima, Y. Honda, O. Kitao, H. Nakai, M. Klene, X. Li, J.E. Knox, H.P. Hratchian, J.B. Cross, C. Adamo, J. Jaramillo, R. Gomperts, R.E. Stratmann, O. Yazyev, A.J. Austin, R. Cammi, C. Pomelli, J.W. Ochterski, P.Y. Ayala, K. Morokuma, G.A. Voth, P. Salvador, J.J. Dannenberg, V.G. Zakrzewski, S. Dapprich, A.D. Daniels, M.C. Strain, O. Farkas, D.K. Malick, A.D. Rabuck, K. Raghavachari, J.B. Foresman, J.V. Ortiz, Q. Cui, A.G. Baboul, S. Clifford, J. Cioslowski, B.B. Stefanov, G. Liu, A. Liashenko, P. Piskorz, I. Komaromi, R.L. Martin, D.J. Fox, T. Keith, M.A. Al-Laham, C.Y. Peng, A. Nanayakkara, M. Challacombe, P.M.W. Gill, B. Johnson, W. Chen, M.W. Wong, C. Gonzalez, J.A. Pople, Gaussian, Inc., Pittsburgh, PA, 2003.
[25] C.L. Campion, W. Li, B.L. Lucht, J. Electrochem. Soc. 152 (2005) A2327.
[26] B. Ravdel, K.M. Abraham, R. Gitzendanner, J. DiCarlo, B. Lucht, C. Campion, J. Power Sources 119–121 (2002) 805.
[27] A. Xiao, L. Yang, B.L. Lucht, Electrochem. Solid State Lett. 10 (2007) A241.
[28] M.Q. Xu, A. Xiao, W.S. Li, B.L. Lucht, Electrochem. Solid State Lett. 12 (2009) A155.
[29] M.Q. Xu, A. Xiao, W.S. Li, B.L. Lucht, J. Electrochem. Soc. 157 (2010) A115.
[30] R. Dedryvere, S. Leroy, H. Martinez, F. Blanchard, D. Lemordant, D. Gonbear, J. Phys. Chem. B 110 (2006) 12986.
[31] Y.S. Hu, W.H. Kong, H. Li, X.J. Huang, Q.L. Chen, Electrochem. Commnu. 6 (2004) 126.
[32] L.E. Ouatani, R. Dedryvere, C. Siret, P. Biensan, D. Gonbeau, J. Electrochem. Soc. 156 (2009) A468.
[33] R. Dedryvere, L. Gireaud, S. Grugeon, S. Laurelle, J.-M. Tarascon, D. Gonbeau, J. Phys. Chem. B 110 (2005) 15868.
[34] D. Aurbach, J. Power Sources 89 (2000) 206.
[35] A.M. Andersson, D.P. Abraham, R. Haasch, S. MacLaren, J. Liu, K. Amine, J. Electrochem. Soc. 149 (2002) A1358.
[36] G.V. Zhuang, H. Yang, P.N. Ross, K. Xu, T.R. Jow, Electrochem. Solid State Lett. 9 (2006) A64.
[37] L. Yang, B. Ravadel, B.L. Lucht, Electrochem. Solid State Lett. 13 (2010) A95.